Chinese Chemical Letters 35 (2024) 109092

Contents lists available at ScienceDirect

Chinese Chemical Letters

journal homepage: www.elsevier.com/locate/cclet

Heptamethine cyanines in bioorthogonal chemistry

Yuanyuan Liao, Yuting Liang, Yurou Huang, Xiaoyan Zeng, Tian He, Jun Yin*

National Key Laboratory of Green Pesticide, International Joint Research Center for Intelligent Biosensor Technology and Health, College of Chemistry, Central China Normal University, Wuhan 430079, China

ARTICLE INFO

Article history:
Received 15 June 2023
Revised 3 September 2023
Accepted 11 September 2023
Available online 13 September 2023

Keywords:
Fluorescent probes
Heptamethine cyanines
Bioorthogonal reaction
Imaging
Cell

ABSTRACT

Due to their excellent fluorescence properties and biological function, cyanine dyes have been widely applied in biological imaging. Heptamethine cyanine (Cy7) dyes, as a type of classic near-infrared (NIR) fluorescent dyes, are considered as one of the effective fluorescent tools in the living organisms due to their good biocompatibility and very low background interference. Bioorthogonal reactions performed in living cells and tissues have developed by leaps and bounds in recent years. The NIR fluorescent labeling technique involving cyanine has attracted widespread attention. This review summarizes their recent application in the field of bioorthogonal imaging, mainly concluding Cy7-type dyes, labeling strategy, bioimaging application, *etc*. We expect this work can provide some helps for the studies of NIR bioorthogonal reaction *in vivo*.

© 2023 Published by Elsevier B.V. on behalf of Chinese Chemical Society and Institute of Materia Medica, Chinese Academy of Medical Sciences.

1. Introduction

Since the 1990s, the idea of conducting chemical reactions in biological systems has emerged to understand the mechanisms behind biological reactions. In 2003, the term "bioorthogonal chemistry" was first introduced by Hang *et al.* in a reaction about the Staudinger ligation within living cells [1–6]. A bioorthogonal reaction is a type of chemical reaction that can take place in an organism without interference from the organism's own chemical reactions [7]. One of its greatest advantage is less toxic to the cell. The bioorthogonal reaction includes two steps: first, the bioorthogonal handle is connected to the biomolecule; second, when a probe or dye with specific functional groups is introduced, the functional group will react with the bioorthogonal handle to successfully achieve the purpose of marking the target biomolecules [8]. Bioorthogonal reactions are widely used in life science, biomedical engineering and clinical medicine, and promotes them greatly [9–16]. Over the last 20 years, the types of reactions have evolved from simple "coupling reactions" to bond coupling, bond breaking, and shear reactions such as Staudinger ligation, strain-promoted azide-alkyne cycloaddition (SPAAC), inverse electron-demand Diels-Alder reaction (IEDDA), copper-mediated azide-alkyne cycloaddition (CuAAC), palladium-mediated Suzuki cross-coupling, ruthenium-mediated olefin metathesis, photo-triggered click reaction (Fig. 1). Additionally, the application scenarios have expanded from a simple living cell system to more complex organisms [17].

Numerous works have confirmed that cyanine dyes have excellent fluorescence imaging behaviors in living biosystems [18–21]. A typical cyanine dye is composed of two nitrogen rings and a $(CH)_n$ conjugate chain within its molecular structure. Consequently, it can serve as fluorescent probes for the detection of biomolecules, fluorescence imaging, and phototherapy [22–38]. Furthermore, modifying the functional groups of the cyanine dyes can adjust their properties and function [39–47]. In recent years, numerous researchers have focused on the use of cyanine dyes in the field of biological orthogonality. They present significant advantages for labeling biomacromolecular substances such as DNA, proteins, and lipids within living cells, enabling visualization of reaction processes in living organisms, and facilitating cellular imaging. Notably, the long conjugate structure of heptamethine cyanine (Cy7) dyes provides strong absorption in the near-infrared (NIR) region, making them particularly suitable for *in vivo* imaging. Cy7, in particular, exhibits superior accumulation and durability, making it particularly advantageous for tumor imaging. This review provides a comprehensive summary of the recent progress on Cy7-type cyanines in bioorthogonal chemistry. It will be greatly helpful for further exploring the application of Cy7 dyes in biological systems.

2. Cy7-based bioorthogonal chemistry

A group led by Lim developed a class of F_{86}Cy dyes in 2020 [48], which are capable of producing the most red-shifted soluble fluorophores. The team obtained the structure of **Cy7–01**

* Corresponding author.
E-mail address: yinj@mail.ccnu.edu.cn (J. Yin).

https://doi.org/10.1016/j.cclet.2023.109092
1001-8417/© 2023 Published by Elsevier B.V. on behalf of Chinese Chemical Society and Institute of Materia Medica, Chinese Academy of Medical Sciences.

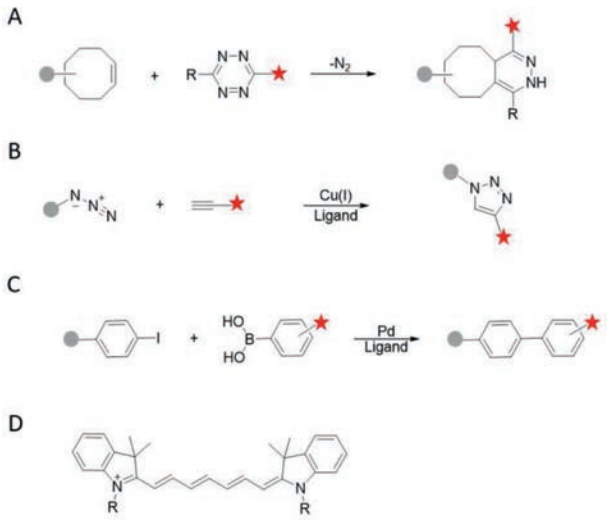

Fig. 1. Representatives of bioorthogonal ligation reaction. (A) Inverse electron-demand DielsAlder reaction (IEDDA). (B) Copper-mediated azide-alkyne cycloaddition (CuAAC). (C) Palladium-mediated Suzuki cross-coupling. (D) The skeleton structure of Cy7.

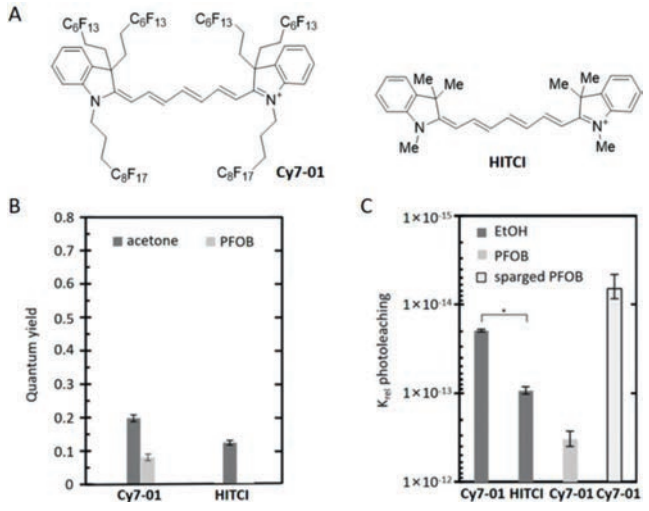

Fig. 2. (A) The structure of **Cy7–01** and **HITCI**. (B) Quantum yields of **Cy7–01** and **HITCI** in acetone and **Cy7–01** in perfluorooctyl bromide (PFOB). (C) Relative photobleaching rates of **Cy7–01** and **HITCI** in EtOH, **Cy7–01** in PFOB, and **Cy7–01** in N_2-sparged PFOB. $^*P < 0.0001$. Reproduced with permission [48]. Copyright 2020, American Chemical Society.

(Fig. 2A) and tested its various properties. The experimental results show that the compound is highly soluble in fluoride solution, acetone and ethanol. By comparing the absorption and emission wavelengths of the fluorinated and nonfluorinated reactions, **Cy7–01** showed a good red-shift phenomenon and the absorption coefficient. Moreover, the fluorescence quantum yield of the fluorinated group is 1.6 times that of the nonfluorinated group (Fig. 2B) and is four times more photostable than its scaffold (Fig. 2C), due to the electron absorption effect of the fluorine. These results highlight the benefit of using a fluorescently-labeled F_{86}Cy dye for imaging. The biorthogonal properties of perfluorocarbons discovered by the team probably provide a new way to introduce dynamic nanodroplets and microdroplets into cells and organisms.

Slikboer *et al.* [49] synthesized a new cyanine dye derived from tetridazine in the same year. This dye **Cy7–02** can serve as a targeted photoacoustic (PA) imaging probe for tumor imaging (Fig. 3A), and it has high albumin binding properties to promote tumor localization and decomposition of cyanine dyes, enhancing its signal output *in vivo*. They conducted *in vivo* and *in vitro* tumor imaging experiments to investigate the effects of this dye on tumor imaging. The fluorescence signal in the tumor was clearly visible one hour after injection of **Cy7–02**, and the uptake of the dye was evident in the *in vitro* imaging of the tumor (Fig. 4A). To image calcium accumulation, they synthesized a novel PA probe, **Cy7–03** (Fig. 3A), using bioorthogonal reactions between **Cy7–02** and *trans*-cyclooctene-bisphosphonate (TCO-BP). TCO-BP targets radiolabeled tetrazines to high calcium accumulation sites. In an *in vivo* calcium accretion imaging study, only the knees of mice with **Cy7–03** showed strong signals (Fig. 4B). Moreover, the authors used inverse electron demand Diels Alder reaction (IEDDA) to link **Cy7–02** to [^{99m}Tc]Tc-TCO-BP (Fig. 3B), to quantitatively determine the systemic biodistribution of PA imaging dyes.

According to the studies conducted, it has been demonstrated that the PA imaging probes developed by Slikboer *et al.* can be effortlessly imaged *in vivo*, and the creation of such probes is uncomplicated. Furthermore, the targeting agent can be replaced in the final stage without a complete resynthesis and optimization of the new complex. This offers a novel way of treating cancer and other ailments.

Even though the far infrared is advantageous over the near infrared, most fluorescent probes currently in existence use tetrazines that are quenched by through-bond energy transfer (TBET) or Forster resonance energy transfer (FRET) between the acceptor and donor fluorophore. However, some fluorescent probes

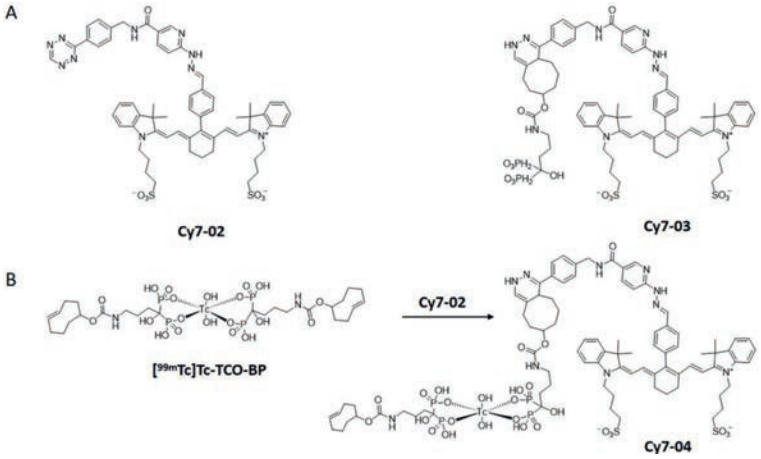

Fig. 3. (A) The structures of **Cy7–02** and **Cy7–03**. (B) The synthesis of **Cy7–04**.

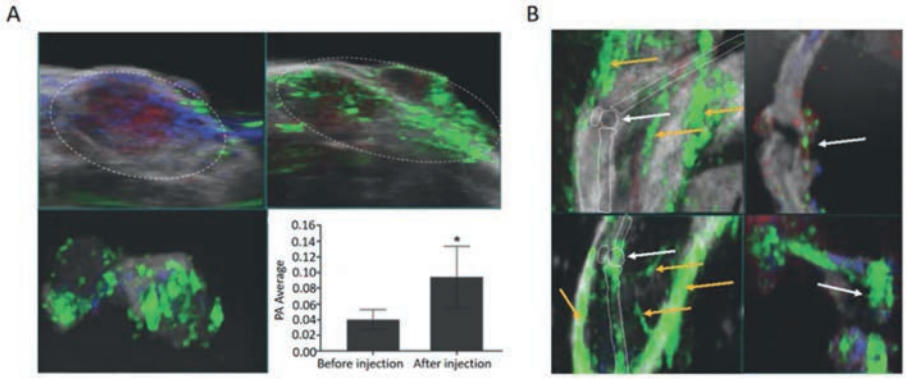

Fig. 4. (A) 143B PA images of human osteosarcoma mouse xenograft tumors injected with **Cy7–02**. (B) PA images of the focused knee joint 1 h after **Cy7–02** injection (top) and **Cy7–03** injection (bottom) are shown *in vitro*. Reproduced with permission [49]. Copyright 2020, American Chemical Society.

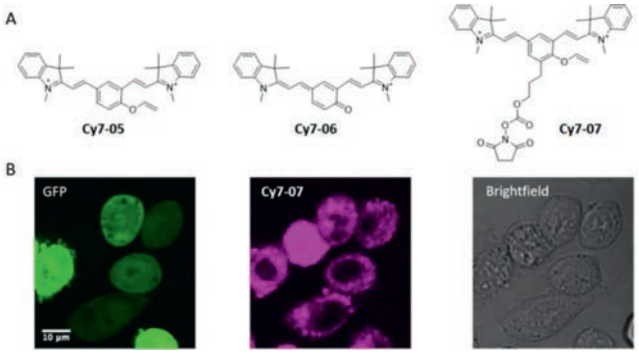

Fig. 5. (A) The structures of **Cy7–05**, **Cy7–06** and **Cy7–07**. (B) RNA probes label cells capable of expressing green fluorescent protein. Reproduced with permission [50]. Copyright 2016, American Chemical Society.

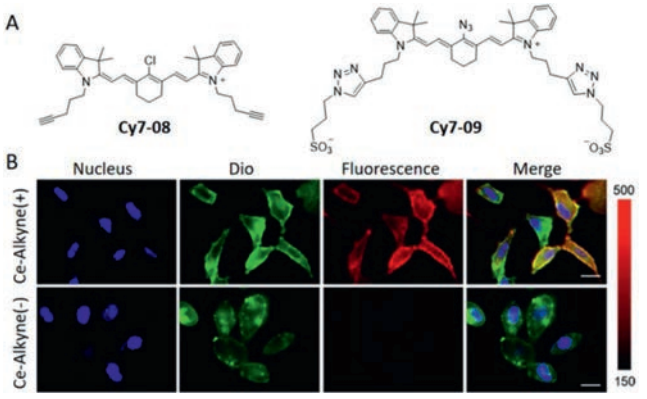

Fig. 6. (A) The structures of **Cy7–08** and **Cy7–09**. (B) A549 cells were imaged with (top) and without (bottom) **Cy7–09** labeling. Reproduced with permission [51]. Copyright 2020, American Chemical Society.

cannot be quenched by tetrazines through energy transfer due to poor overlap with the far-infrared spectrum. In 2016, Wu *et al.* [50] developed a near-infrared fluorescent probe for tetrazine reactions that uses an alternative quenching mechanism. The team employed an internal charge transfer (ICT) process to quench the fluorophore, and the quenched ICT fluorophore can be revealed using a bioorthogonal click release strategy.

To determine the design strategy of probes, the authors first prepared **Cy7–06** using the compound **Cy7–05** (Fig. 5A). Upon adding **Cy7–05** and **Cy7–06** to the phosphate buffer saline (PBS) solution, the fluorescence intensity of **Cy7–06** was 70 times greater than that of **Cy7–05**. Additionally, the transfer of the absorption peak of **Cy7–06** from 620 nm to 560 nm after capturing it with vinyl ether confirms the logic of the ICT process. Next, the authors synthesized **Cy7–07** (Fig. 5A) and linked it to RNA to create a probe. Finally, the team used RNA probes to label RNA in cells and imaged the cells (Fig. 5B). This new mechanism can be applied to a wider range of fluorescent preparations.

Constructing NIR probes with multiple functional components is challenging due to the instability of common NIR dyes. However, researchers are actively exploring solutions in this field. In 2020, Wang *et al.* [51] developed a novel NIR scaffold with three clickable handles, which exhibited favorable fluorescence properties when connected to different biomolecules. The authors utilized this scaffold to design **Cy7–09** (Fig. 6A), which was applied to A549 cells expressing cetuximab. The experimental results demonstrated that **Cy7–09** enabled cells with terminal alkyne groups on the cell membrane to exhibit bright NIR signals (Fig. 6B), achieving *in situ* NIR labeling of antibodies on the surface of living cells. Additionally, the authors designed NIR-positron emission tomography (PET) dual-modal probes for *in vivo* tumor imaging to address the challenge of introducing radiotracers with short half-lives. The authors synthesized **Cy7–10** (Fig. 7A) and employed the probe to image U87MG tumors in naked mice, revealing a strong fluorescent signal (Fig. 7B) at the tumor site. This unique scaffold with three clickable handles and continuous click reactions under biocompatibility conditions successfully resolved the issue of building NIR probes with multiple biofunctional arms.

In certain cases, some reagents cannot dissolve in water and need organic reagents at higher concentrations, otherwise their activity may decrease, or they may become more vulnerable to high temperatures. In 2016, Rodriguez [52] developed a probe that is highly water-soluble and compatible with multimode imaging. They connected the boron fluoride trap derivative to Cy7 through a bioorthogonal ligation method to obtain a multimodal imaging probe capable of [^{18}F]-PET and near-infrared fluorescent (NIRF) imaging (Fig. 8).

Streptavidin-agarose was employed as a solid carrier for the probe after it was conjugated to the antibody. The use of fluoride aqueous solution enabled the elution of the probe, **Cy7–11**, from the solid phase, yielding free **Cy7–12** for tracking the antibody (Figs. 9A and B). The residual **Cy7–11** could be reserved for future use. The substrate could be recycled for multiple synthesis cycles by simply rinsing it with [^{18}F]-fluoride. Additionally, the probe-antibody complex that remained uneluted by [^{18}F]-fluoride stayed in the solid phase, ensuring the purity of the probe in the solution and increasing its specific activity.

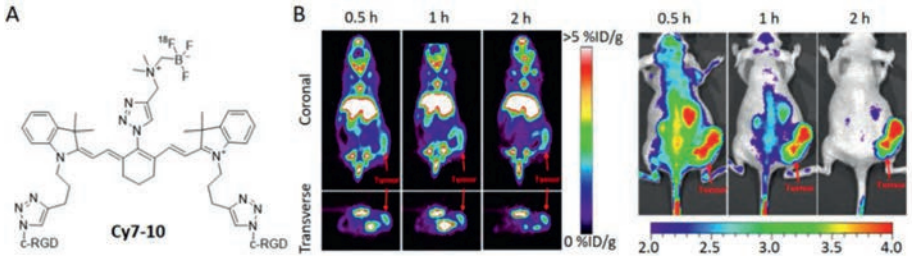

Fig. 7. (A) The structure of **Cy7–10**. (B) PET images (left) and fluorescent images (right) of U87MG tumor xenograft mice obtained at different times after intravenous injection of **Cy7–10**. Reproduced with permission [51]. Copyright 2020, American Chemical Society.

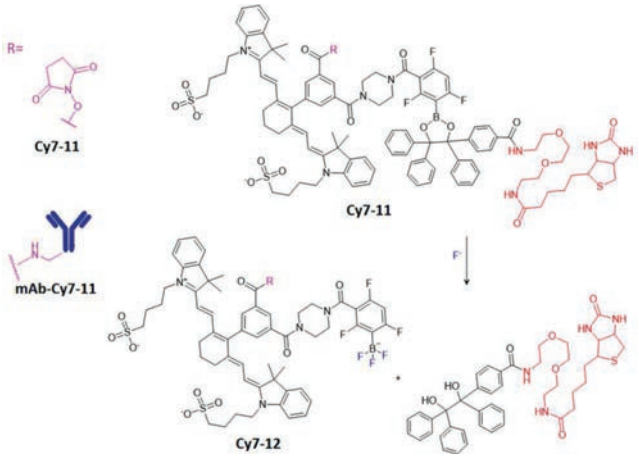

Fig. 8. The structural formulas of **Cy7–11** and **Cy7–12** are shown in the figure. By washing with [^{18}F]-fluorine, **Cy7–11** can be decomposed into **Cy7–12** and separated from the solid carrier.

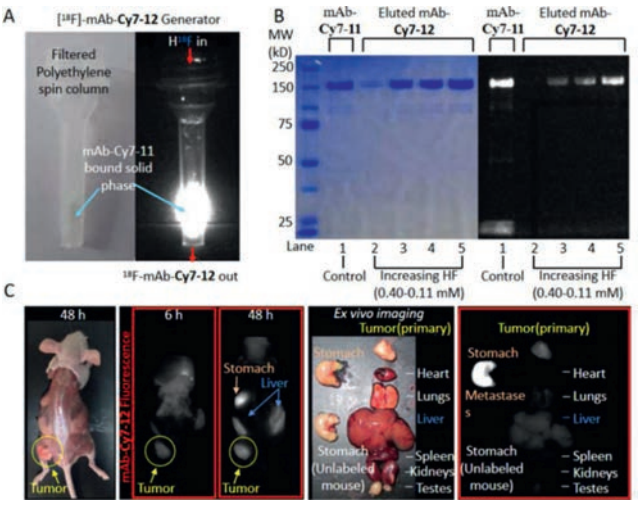

Fig. 9. (A) Imaging of streptavidin-agarose-solid rotating column containing biotin-mAb-**Cy7–11** under bright conditions and fluorescence. (B) mAb-**Cy7–11** and mAb-**Cy7–12** analyzed by sodium dodecyl sulfate polyacrylamide gel electrophoresis (SDS-PAGE). (C) Image of [^{19}F]-mAb-**Cy7–12** in the primary tumor and stomach at 6 h and 48 h, respectively. Reproduced with permission [52]. Copyright 2016, American Chemical Society.

The probe takes advantage of both solid phase tracer generation and the unique attenuation properties of [^{18}F]-PET nuclides, resulting in a superior PET/NIRF multimodal imaging approach. This approach offers improved depth-of-penetration, spatial resolution, and temporal resolution when compared to a simple multi-

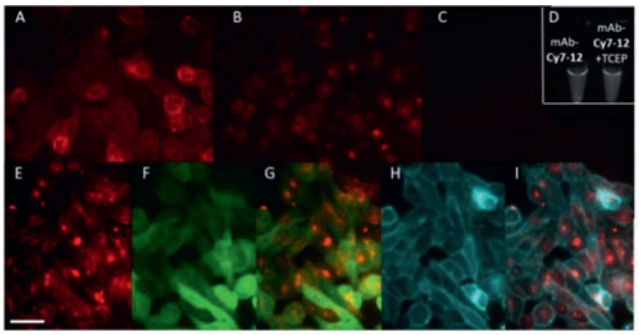

Fig. 10. Imaging of [^{18}F]-mAb-**Cy7–12** and [^{19}F]-mAb-**Cy7–12** under a variety of controlled conditions. Reproduced with permission [52]. Copyright 2016, American Chemical Society.

modal response. Additionally, the mild solid adhesion and fluorine-induced decomposition of aryl dioxyborane do not impact antigen-specific binding, allowing for the targeting of more complex biological targets. By using monoclonal antibody (mAb), this probe eliminates the need to separate multiple active species and does not require high radiochemical yields like traditional markers. Antigen-binding is unaffected by chemical attachment, solid carrier solidation, or fluorine-containing solvent elution, as demonstrated by images of [^{18}F]-mAb-**Cy7–12** and [^{19}F]-mAb-**Cy7–12** under controlled conditions (Fig. 10).

Once the results are obtained, it is necessary to verify the binding of the antigen. In the experimental group, PC3 cells were labeled with [^{19}F]-mAb-**Cy7–12** and then rinsed with unlabeled mAb, resulting in a significant reduction in membrane fluorescence, thus confirming the specificity of the [^{19}F]-mAb-**Cy7–12** membrane binding to the antigen (Figs. 10A and B). Although the weight of the [^{19}F]-mAb-**Cy7–12** was reduced by TCEP, resulting in severe fluorescence loss, the monoclonal antibodies used in this study (Figs. 10A and C) showed equivalent Cy7 fluorescence through other pathways, indicating that the binding of [^{19}F]-mAb-**Cy7–12** to the antigen was necessary for endogenous fluorescence (Figs. 10C and D). The experimental group incubated the cells for a longer time (Fig. 10E), and performed fluorescent imaging of the cytoplasm and cell membranes with red fluorescent protein (RFP) and DiO membrane dye, respectively. The imaging results were superimposed with Fig. 10E to obtain Figs. 10F–I. The experimental results confirmed that increasing the incubation time could promote endocytosis. Furthermore, the experimental group demonstrated that [^{19}F]-mAb-**Cy7–12** can perform fluorescence imaging *in vivo* at short time points and can be used to monitor tumor metastasis (Fig. 9C).

The fluorescence of current tetraazine-based bioorthogonal probes decreases significantly as their emission wavelength shifts to the NIR region, severely limiting their applicability in living cells

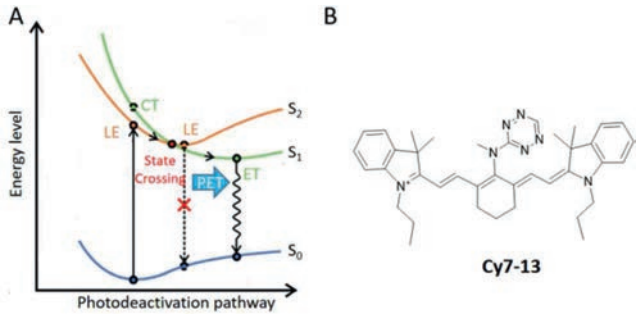

Fig. 11. (A) The PET process is represented by the state-crossing from a Locally Excited to an Electron Transfer State (SLEET) model. (B) The structure of **Cy7–13**. Note: ET for the electron transfer state; CT for the charge transfer state; LE for the locally excited state. Reproduced with permission [54]. Copyright 2021, American Chemical Society.

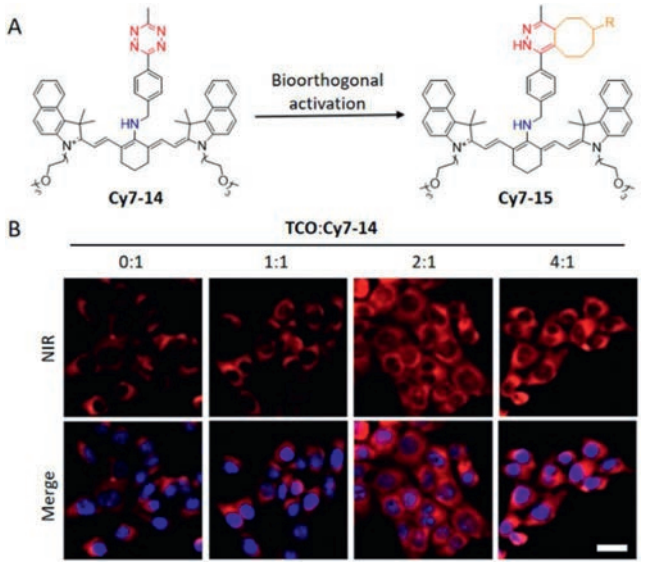

Fig. 12. (A) The structures of **Cy7–14** and **Cy7–15**. (B) Confocal laser scanning microscopy (CLSM) imaging in 4T1 cells after different concentrations of TCO treated with **Cy7–14**. Reproduced with permission [55]. Copyright 2022, Springer Nature.

and tissues. However, in 2022, Mao and colleagues [53] utilized the photoinduced electron transfer mechanism (Fig. 11A) [54] to reduce background fluorescence and created a series of tetrazine-based far red/NIR fluorescent dyes with outstanding performance at longer wavelengths. One of these dyes, **Cy7–13** (Fig. 11B), was synthesized by the authors and its fluorescence quenching was attributed to the photoinduced electron transfer mechanism. The probes produced through this technique are highly biocompatible and photostable, making them well-suited for imaging specific intracellular targets and tumors *in vivo*.

Recently, a new strategy for designing cyanine dyes for tumor imaging was developed by Zhang *et al.* in 2022 [55]. They utilized the torsion-induced disaggregation (TIDA) phenomenon to design **Cy7–14**, which was then connected to tetrazine-transcyclooctene (Tz-TCO) to generate **Cy7–15** (Fig. 12A). The conformational change of the fluorophore's heptamethyl chain from S-*trans* to S-*cis* resulted in significant fluorescence enhancement, making the molecule ideal for tumor imaging. The authors successfully used **Cy7–14** for live-cell imaging and in a 4T1 tumor-bearing mouse model, as shown in Fig. 12B and Fig. 13, respectively, confirming its effectiveness for enhancing fluorescent signal and imaging tumors.

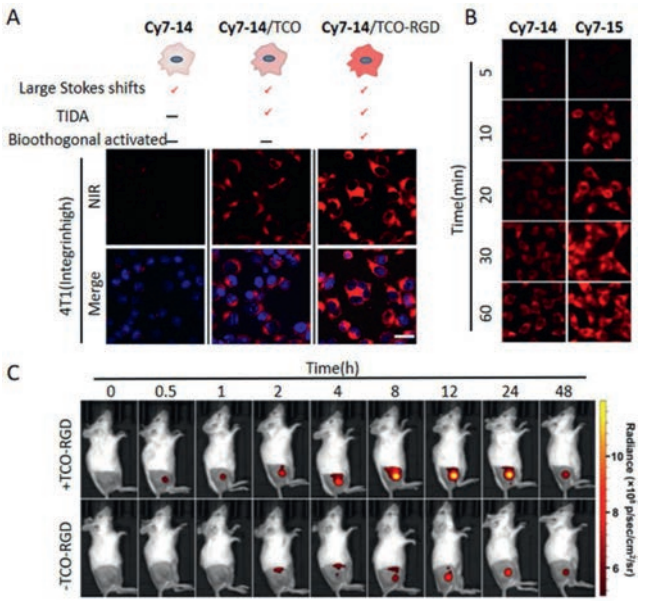

Fig. 13. (A) CLSM imaging of 4T1 cells with **Cy7–14** under different conditions. (B) Confocal fluorescence images of **Cy7–14** and **Cy7–15** in 4T1 cells. (C) NIR imaging of mouse tumors injected with RGD-TCO and **Cy7–14**. Reproduced with permission [55]. Copyright 2022, Springer Nature.

Cy7 is frequently utilized as a fluorescent reagent in fluorescence imaging due to its exceptional biocompatibility and NIR fluorescence qualities. Fluorescence imaging can be employed for visualization in the antibody-drug conjugate (ADC) approach, utilizing photochemical properties. In 2017, Nani [56] demonstrated that the compound **Cy7–16** (Fig. 14A) facilitated small molecule release under light irradiation within the 690 nm range. However, the compound requires improvement for clinical use. Firstly, the modification structure of the original compound should be altered to increase its λ_{max}, as the excitation wavelength is still relatively far from the near infrared band. Secondly, the scaffold of the initial compound must be enhanced to address the background hydrolysis effect, strengthen photooxidation, increase the effectiveness of the payload molecule, and realize high-strength labeling.

After a series of explorations, the team identified **Cy7–17a** and **Cy7–17b** (Fig. 14A) as potential small molecule delivery agents that required further evaluation. These compounds exhibited high red-shifts and significantly reduced background hydrolysis effects. To improve efficacy and simplify conjugation processes, the team utilized bioorthogonal reactions to modify the **Cy7–17a** and **Cy7–17b** scaffolds and coupled them with panitumumab, a monoclonal anti-EGFR antibody commonly used in clinical settings, resulting in the final target molecules **Cy7–18a** and **Cy7–18b** (Fig. 14A). **Cy7–18b** was found to possess a better therapeutic index and NIR photosensitivity under identical light source conditions and was therefore selected for *in vivo* studies. Subsequently, the team evaluated the *in vivo* efficacy of **Cy7–18b** in mice bearing MDA-MB-468-luc tumors. Through fluorescence imaging and luminescence imaging of luciferase activity (Figs. 14B and C), they discovered that the drug was well-tolerated by mice and inhibited tumor proliferation. This approach provides a unique platform for cyanine scaffold remodeling to target drug delivery and offers new possibilities for treating diseases.

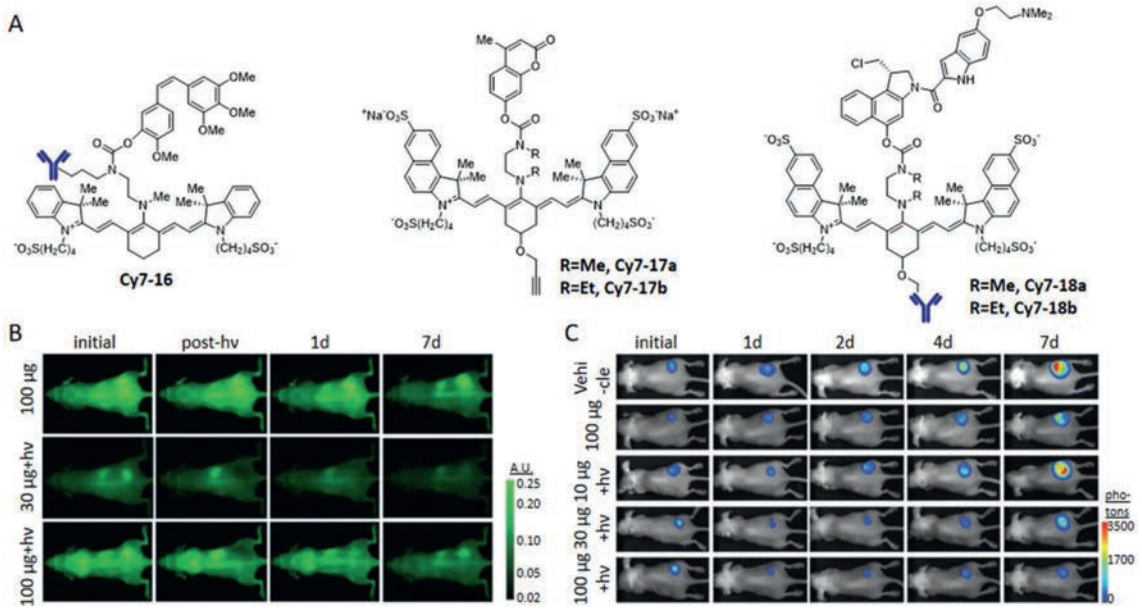

Fig. 14. (A) The structures of **Cy7–16**, **Cy7–17** and **Cy7–18**. (B) Fluorescence images at 800 nm. (C) Bioluminescence images of luciferase activity. Reproduced with permission [56]. Copyright 2017, American Chemical Society.

3. Conclusion

In conclusion, this review provides a comprehensive summary of the current applications of Cy7-type dyes in the field of bioorthogonal chemistry in terms of dye molecular structure, reaction conditions, fluorescence imaging, and bioapplications. Although Cy7-type dyes demonstrate unparalleled biocompatibility and excellent bioimaging performance in living cell, tissue and *in vivo*, their disadvantages in terms of photostability, fluorescence quantum yields, and toxicity remain the greatest barriers to their further application. These are still the directions we need to work on in the coming research. Furthermore, to further enhance their function and applications, some Cy7-type dyes with novel backbones will be developed and used in the future, especially those with more functionalization sites, which will provide more options for bioorthogonal chemistry. We also believe that bioorthogonal reactions with NIR fluorescence characteristics will be increasingly used in living organisms [57–60]. In particular, it will play an increasingly important role in exploring the functions of various biomolecules in cellular and physiopathological processes, and clinical diagnosis and treatment.

Declaration of competing interest

The authors declare that they have no known competing financial interests or personal relationships that could have appeared to influence the work reported in this paper.

Acknowledgments

This work was supported by the National Key R&D Program of China (No. 2022YFA1207400), National Natural Science Foundation of China (No. 22274061), the 111 Project (No. B17019) and Fundamental Research Funds for the Central Universities (No. CCNU22QN007).

References

[1] H. Hang, C. Yu, D. Kato, C. Bertozzi, Proc. Natl. Acad. Sci. U. S. A. 100 (2003) 14846–14851.
[2] J. Li, P. Chen, Nat. Chem. Biol. 12 (2016) 129–137.
[3] S. Nguyen, J. Prescher, Nat. Rev. Chem. 4 (2020) 476–489.
[4] T. Deb, J. Tu, R. Franzini, Chem. Rev. 121 (2021) 6850–6914.
[5] A. Battigelli, B. Almeida, A. Shukla, Bioconjug. Chem. 33 (2022) 263–271.
[6] L. Taiariol, C. Chaix, C. Farre, E. Moreau, Chem. Rev. 122 (2022) 340–384.
[7] D. Patterson, L. Nazarova, J. Prescher, ACS Chem. Biol. 9 (2014) 592–605.
[8] R. Das, J. Hardie, B. Joshi, et al., JACS Au 2 (2022) 1679–1685.
[9] R. Bird, S. Lemmel, X. Yu, Q. Zhou, Bioconjug. Chem. 32 (2021) 2457–2479.
[10] S.Y. Chow, A. Unciti-Broceta, JACS Au 2 (2022) 1747–1756.
[11] B. Akgun, D. Hall, Angew. Chem. Int. Ed. 57 (2018) 13028–13044.
[12] K. Lo, Acc. Chem. Res. 53 (2020) 32–44.
[13] J. Li, H. Kong, C. Zhu, Y. Zhang, Chem. Sci. 11 (2020) 3390–3396.
[14] A. Lossouarn, P.Y. Renard, C. Sabot, Bioconjug. Chem. 32 (2021) 63–72.
[15] D. Bilodeau, K. Margison, M. Serhan, J. Pezacki, Chem. Rev. 121 (2021) 6699–6717.
[16] T. Heiss, R. Dorn, J. Prescher, Chem. Rev. 121 (2021) 6802–6849.
[17] J. Prescher, C. Bertozzi, Nat. Chem. Biol. 1 (2005) 13–21.
[18] E.M.S. Stennett, M.A. Ciuba, M. Levitus, Chem. Soc. Rev. 43 (2014) 1057–1075.
[19] W. Sun, S. Guo, C. Hu, et al., Chem. Rev. 116 (2016) 7768–7817.
[20] G. Fei, S. Ma, C. Wang, et al., Coordin. Chem. Rev. 447 (2021) 214134.
[21] N.G. Medeiros, C.A. Braga, V.S. Câmara, et al., Asian J. Org. Chem. 11 (2022) e202200095.
[22] H. Chen, W. Chen, Y. Lin, et al., Chin. Chem. Lett. 32 (2021) 2359–2368.
[23] W. Chen, X. Ma, H. Chen, et al., Coordin. Chem. Rev. 427 (2021) 213584.
[24] Y. He, S. Liu, J. Yin, J. Yoon, Coordin. Chem. Rev. 429 (2021) 213610.
[25] Y. Huang, W. Chen, J. Chung, et al., Chem. Soc. Rev. 50 (2021) 7725–7744.
[26] X. Zeng, W. Chen, C. Liu, et al., J. Agric. Food Chem. 69 (2021) 13700–13712.
[27] X. Liu, Adv. Agrochem 2 (2023) 1–2.
[28] X. Zeng, Y. Huang, J. Dong, et al., Adv. Agrochem 1 (2022) 73–84.
[29] W. Chen, C. Zhang, H. Chen, Anal. Chem. 93 (2021) 3378–3385.
[30] N. Kwon, C. Lim, G. Ko, et al., Anal. Chem. 93 (2021) 11612–11616.
[31] W. Chen, H. Chen, Y. Huang, et al., ACS Appl. Bio Mater. 5 (2022) 3428–3437.
[32] G. Li, J. Wang, D. Li, et al., Chin. Chem. Lett. 32 (2021) 1527–1531.
[33] X. Ma, W. Chi, X. Han, et al., Chin. Chem. Lett. 32 (2021) 1790–1794.
[34] X. Wu, D. Li, J. Li, et al., Chin. Chem. Lett. 32 (2021) 1937–1941.
[35] Z. Li, X. Gao, H. Zhang, et al., Chin. Chem. Lett. 34 (2023) 107645.
[36] Z. Li, S. Chen, Y. Huang, et al., Chem. Eng. J. 450 (2022) 138087.
[37] S. Shen, W. Xu, J. Lu, et al., Chin. Chem. Lett. 35 (2024) 108360.
[38] H. Zhang, C. He, L. Shen, et al., Chin. Chem. Lett. 34 (2023) 108160.
[39] Z. Xu, X. Huang, M. Zhang, et al., Anal. Chem. 91 (2019) 11343–11348.
[40] X. Deng, X. Ma, W. Zhang, et al., Anal. Chim. Acta 1255 (2023) 341118.
[41] X. Ma, Y. Huang, W. Chen, et al., Angew. Chem. Int. Ed. 62 (2023) e202216109.
[42] X. Ma, Y. Huang, S. Abedi, et al., CCS Chem. 4 (2022) 1961–1976.
[43] Z. Xu, X. Huang, X. Han, et al., Chem 4 (2018) 1609–1628.
[44] X. Ma, C. Zhang, L. Feng, et al., J. Mater. Chem. B 8 (2020) 9906.
[45] G. Li, Y. Guan, F. Ye, et al., Spectrochim. Acta A Mol. Biomol. 239 (2020) 118465.
[46] Z. Xu, M. Zhang, Y. Xu, et al., Sens. Actuator. B: Chem. 290 (2019) 676–683.
[47] S. Usama, K. Burgess, Acc. Chem. Res. 54 (2021) 2121–2131.
[48] I. Lim, A. Vian, H. van de Wouw, et al., J. Am. Chem. Soc. 142 (2020) 16072–16081.
[49] S. Slikboer, Z. Naperstkow, N. Janzen, et al., Mol. Pharm. 17 (2020) 3369–3377.
[50] H. Wu, S. Alexander, S. Jin, N. Devaraj, J. Am. Chem. Soc. 138 (2016) 11429–11432.

[51] Y. Wang, J. Weng, J. Lin, et al., J. Am. Chem. Soc. 142 (2020) 2787–2794.
[52] E.A. Rodriguez, Y. Wang, J.L. Crisp, et al., Bioconjug. Chem. 27 (2016) 1390–1399.
[53] W. Mao, W. Chi, X. He, et al., Angew. Chem. Int. Ed. 61 (2022) e202117386.
[54] X. Zhao, Q. Yao, S. Long, et al., J. Am. Chem. Soc. 143 (2021) 12345–12354.
[55] X. Zhang, J. Gao, Y. Tang, et al., Nat. Commun. 13 (2022) 3513.
[56] R.R. Nani, A.P. Gorka, T. Nagaya, et al., ACS Cent. Sci. 3 (2017) 329–337.
[57] V. Pansare, S. Hejazi, W. Faenza, et al., Chem. Mat. 24 (2012) 812–827.
[58] A. Potharazu, A. Gangemi, Int. J. Med. Robot. 19 (2023) e2485.
[59] D. Li, T. Shen, X. Xue, et al., Sci. China Chem. 66 (2023) 2329–2338.
[60] R.Q. Yang, K.L. Lou, P.Y. Wang, et al., Small Methods 5 (2021) e2001066.